Available online at www.sciencedirect.com
ScienceDirect
Energy Reports 9 (2023) 85–93
www.elsevier.com/locate/egyr

2022 The 3rd International Conference on Power and Electrical Engineering (ICPEE 2022)
29–31 December, Singapore

Low-flow ocean current turbine diffuser shroud concentrated and accelerated flow technical research

Hongbo Wei*, Wenbin Su

School of Mechanical Engineering, Xi'an Jiaotong University, Xi'an 710049, Shaanxi, China

Received 13 April 2023; accepted 19 May 2023
Available online xxxx

Abstract

Ocean current energy is the kinetic energy of seawater flow and is a low-cost, low-carbon, clean, and renewable energy source. Ocean current energy is mainly captured by the Ocean Current Turbine (OCT). However, as the depth of the water increases, the flow rate of the water decreases significantly. The main purpose of this paper is to study the low efficiency of current turbine capture due to low current velocities, with the main objective of achieving the effect of gathering and increasing the speed of low current energy. Firstly, this paper investigates the mechanism and mathematical model of the concentrated and accelerated flow of the diffuser shroud. Secondly, the velocity and pressure flow fields of the basic diffuser shroud are simulated and analyzed under different low flow velocity conditions (flow velocity below 1.0 m/s), different aspect ratios, and different diffusion opening angles. This paper further investigates the effect of speed increase for four different airfoil sections of diffuser shroud. Finally, measurements and verification are carried out with Particle Image Velocimetry (PIV) circular water hole experiments. The experimental results demonstrate the concentrated and accelerated results of the diffuser shroud. The basic diffuser shroud has a 39% increase in flow field velocity. The airfoil section diffuser shroud has a better velocity increase on the flow field than the basic diffuser shroud. The flow field flow rate increased to 58%. The optimum location for the speed increase is near the inlet and less than 0.5 times the inlet diameter. Compared to the simulation results, the experimental results of the PIV circulating water hole show an average error of less than 4%. The results of this paper provide a research basis for the efficient capture of current energy in deep-sea low-flow waters and a theoretical basis for the design of low-flow current energy turbines.

Peer-review under responsibility of the scientific committee of the 3rd International Conference on Power and Electrical Engineering, ICPEE, 2022.

Keywords: Ocean current energy; Diffuser shroud; Highly efficient energy capture; Low velocity current energy

1. Introduction

The gases produced by burning fossil energy sources such as coal and oil not only cause extreme weather such as haze, but they also upset the ecological balance and contribute to the greenhouse effect, which can lead

* Corresponding author.
E-mail address: whb1427@stu.xjtu.edu.cn (H. Wei).

https://doi.org/10.1016/j.egyr.2023.05.100

Peer-review under responsibility of the scientific committee of the 3rd International Conference on Power and Electrical Engineering, ICPEE, 2022.

to an economic and ecological collapse in severe cases [1–3]. Moreover, excessive dependence on fossil energy sources can produce a homogeneous form of the energy mix, while leading to the fragility and instability of state power [4–6]. Amongst other things, clean and sustainable ocean energy is the main focus of renewable energy researchers [7,8].

Ocean energy is a renewable resource found in the ocean, with abundant reserves and wide distribution [9]. One of the most important forms of ocean energy is ocean current energy. Ocean current energy is the kinetic energy of seawater currents, and also is an almost ubiquitous and inexhaustible source of marine renewable energy [10].

The main form of ocean current energy capture is the ocean current turbine [11,12]. OCT can be classified into two main types according to rotor configurations: horizontal axis ocean current turbines and vertical axis ocean current turbines [13], as seen in Fig. 1. The main form is the horizontal axis current energy turbine [14].

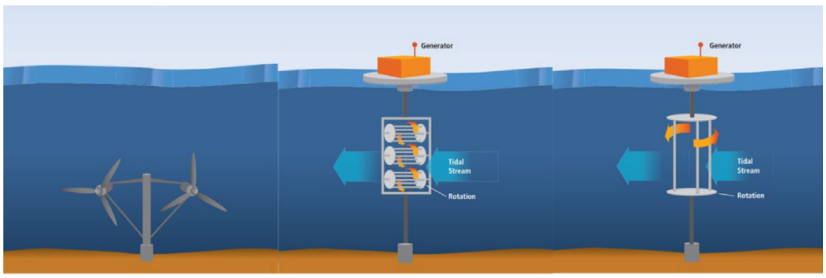

Fig. 1. Ocean current energy converters. (a) twin turbine horizontal axis device. (b) cross-flow device. (c) vertical axis device. (design by NREL).

However, for current energy, the maximum current velocity in most waters is only 2 m/s at water depths less than 200 m, and 0.5 m/s at 1000 m, while the average current velocity is much less than this value. Current velocities are generally low in most waters, and as water depth increases, current profile velocities drop rapidly and flow direction changes are complex, limiting the efficiency of current energy capture.

If the ocean energy can be locally concentrated, the power output of the OCT can be significantly increased [15,16]. Currently the speed and power of the OCT is mainly increased by means of a diffuser mounted at the end of the rotor [17], as shown in Fig. 2.

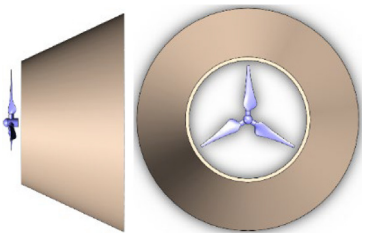

Fig. 2. Diffuser-augmented ocean current turbine.

Particle Image Velocimetry (PIV) enables flow field measurements to be made on the diffuser shroud. For research and diagnostics into flow, turbulence, microfluidics, spray atomization, and combustion processes, PIV is a non-intrusive laser optical monitoring tool [18].

The main research of this paper includes the following aspects. Firstly, the mathematical model and hydrodynamic characteristic equations of diffuser shroud are established. Secondly, the velocity and pressure flow fields of the diffuser shroud at different flow velocities, different aspect ratios, different diffusion opening angles and different airfoil cross-sections are simulated by the CFD simulation software Fluent. Finally, in order to verify the simulation results, flow field experiments were carried out on the 3D printed diffuser shroud at low flow velocity of 0.7 m/s through a PIV recirculating water cave.

2. Diffuser shroud flow acceleration mechanism

In this paper, the velocity of a local flow field is increased by designing a flow field velocity increasing structure. The basic idea is to increase the velocity of the local flow field by changing the area of the fluid flowing through the cross section to achieve a change in pressure in the flow field. The fluid gains energy from being pushed by pressure as follows:

$$F_1 s_1 - F_2 s_2 = p_1 A_1 v_1 \Delta t - p_2 A_2 v_2 \Delta t \tag{1}$$

According to the law of conservation of energy, the energy gained by the fluid due to the force + the energy lost by the fluid due to the work done by gravity = the kinetic energy gained by the fluid.

$$p_1 A_1 v_1 \Delta t - p_2 A_2 v_2 \Delta t + \rho g A_1 v_1 \Delta t h_1 - \rho g A_2 v_2 \Delta t h_2 = \frac{1}{2}\rho A_2 v_2 \Delta t v_2^2 - \frac{1}{2}\rho A_1 v_1 \Delta t v_1^2 \tag{2}$$

In the area with the smallest cross-sectional area, the static pressure reaches its minimum value, resulting in a pressure differential that leads to an increase in flow velocity in this area. Based on these findings, a diffuser shroud with a small inlet area and a large outlet area can be designed. diffuser shroud is used as a flow field velocity increasing structure to increase the flow velocity at the inlet, as shown in Fig. 3.

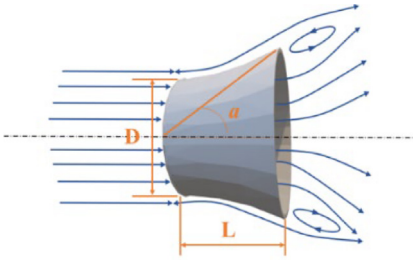

Fig. 3. Schematic diagram of the flow field around diffuser shroud.

3. Diffuser shroud design and analysis

The Basic diffuser shroud is a diffusion profile that increases the velocity of the fluid by means of an inlet diameter smaller than the outlet diameter. The diffuser achieves high performance by adjusting parameters such as the length-to-diameter ratio (L/D), the diffusion opening angle (a) and the shape of the cross-section to achieve a high-performance flow velocity increase, as shown in Fig. 4.

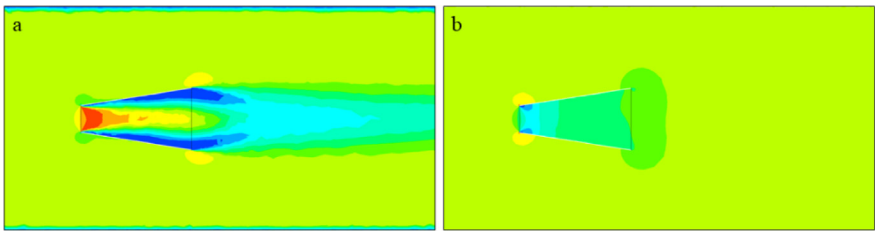

Fig. 4. Flow field of the diffuser shroud at L/D = 4. (a) velocity contour; (b) pressure contour.

3.1. The effect of L/D on the flow field

The length-to-diameter ratio L/D of the basic diffuser shroud is the basic parameter of the diffuser shroud. Under the condition that the inlet diameter of the deflector D = 170 mm and the diffusion opening angle a = 9° are constant, the flow field is simulated and analyzed for four different aspect ratios (L/D = 0.5, 1, 2, 4). As an example, the simulation results for L/D = 4 are shown in Fig. 4.

For comparison purposes, the flow velocity and pressure flow field simulation results of the diffuser shroud are compared for four aspect ratios, as shown in Fig. 5. X/L represents the axial position ratio of the diffuser shroud.

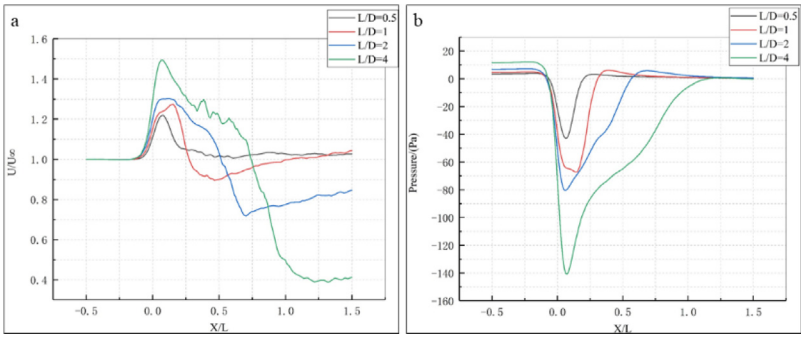

Fig. 5. Velocity and pressure curves for basic diffuser shroud at different aspect ratios. (a) velocity curves; (b) pressure curves.

As shown in Fig. 5, the optimum location for the incremental velocity of the basic diffuser shroud convective field is near its inlet region (i.e. near X/L = 0.2 to 0.3). The optimum coefficients of increase for the diffuser shroud to flow field velocity are 1.2187, 1.2746, 1.3023 and 1.4939 for L/D = 0.5, 1, 2 and 4 respectively.

3.2. The effect of diffusion opening angle on the flow field

The diffuser shroud inlet diameter D = 170 mm and the length-to-diameter ratio D/L = 1 are fixed, but the value of the diffusion opening angle a is changed in this paper. CFD simulations are carried out for a = 7°, 9°, 10°, 15° and 25°. We can obtain five separate sets of flow field pressure and velocity distributions. In this paper, the simulation results for a diffusion opening angle of 15° are shown as an example in Fig. 6.

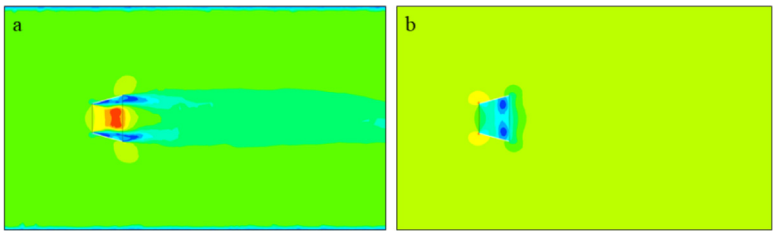

Fig. 6. Flow field of diffuser shroud at a = 15°. (a) velocity contour; (b) pressure contour.

As shown in Fig. 7(a), the basic diffuser shroud has the best speed increase at a diffusion opening angle of 15°. At an X/L position of 0.1331, the speed increase factor can reach 1.3882. Similarly, as shown in Fig. 7(b), at an inclination angle of a = 15°, the diffuser shroud has the lowest pressure at the X/L position of 0.1331. As the diffuser opening angle increases, the effect of the diffuser shroud velocity increase does not necessarily increase.

3.3. The effect of airfoil cross-section on flow field

In this paper, a simulation study is carried out on a diffuser shroud with a NACA airfoil cross-section. The key structural factor that determines the shape of this diffuser shroud is the airfoil parameter. This key structural factor influences the shape of the airfoil cross-sectional, as well as the effect of the diffuser on the velocity increase of the local flow field and the location of the velocity increase. The flow field of a diffuser with four different airfoil cross-sections is discussed for an inlet diameter of L = 170 mm, a length-to-diameter ratio of D/L = 2 and a diffusion opening angle of a = 15°. The four wing sections are NACA4412, NACA2412, NACA1412 and NACA2410. The simulation results for the NACA2412 wing section are shown in Fig. 8 as an example.

The velocity profile and pressure profile on the centerline of the diffuser shroud for different airfoil sections are shown in Fig. 9. the NACA4412 airfoil section achieves a speed increase coefficient of 1.627 at X/L = 0.221. the NACA4412 airfoil has a high lift to resistance ratio characteristic, which may explain its large speed increase

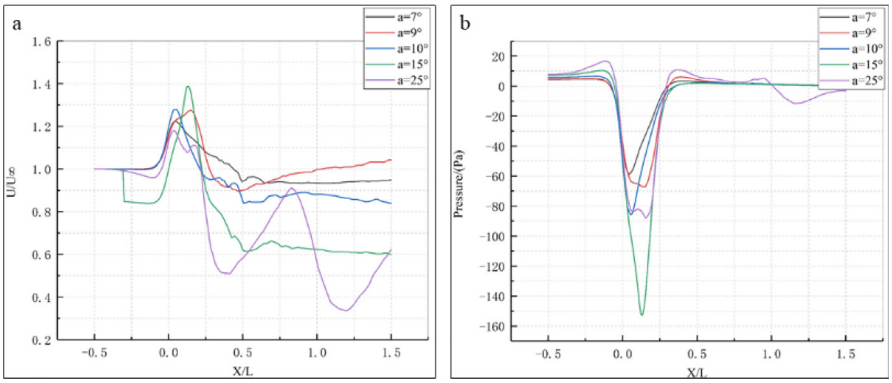

Fig. 7. Velocity and pressure curves for basic diffuser shroud with different diffusion opening angles. (a) velocity curves; (b) pressure curves.

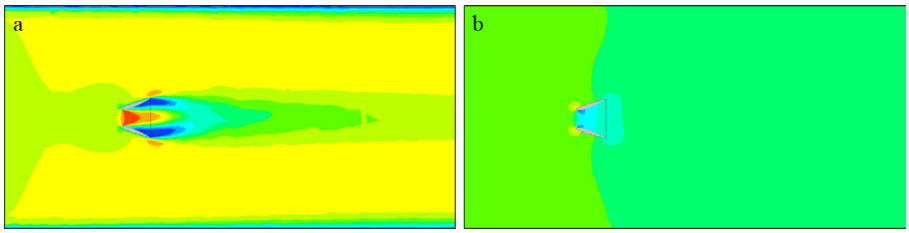

Fig. 8. Flow field of the diffuser shroud of the NACA2412 airfoil section. (a) velocity contour; (b) pressure contour.

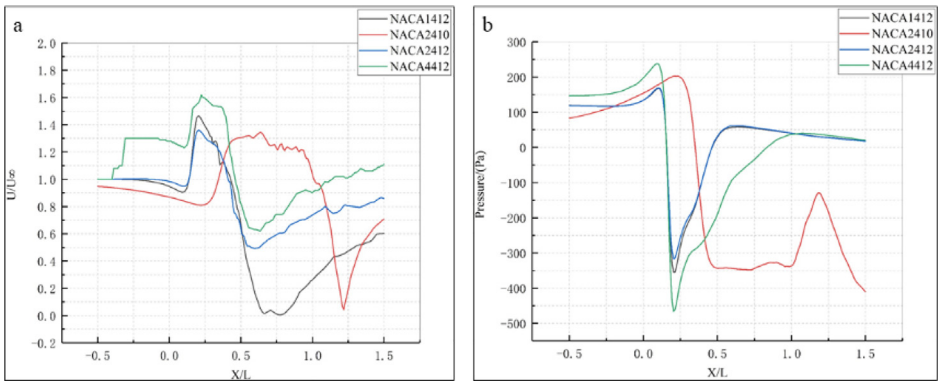

Fig. 9. Velocity and pressure curves for diffuser shroud with different airfoil sections. (a) velocity curves; (b) pressure curves.

coefficient. Due to the more complex airfoil parameters, the speed increase and pressure drop coefficients show great fluctuations from one airfoil to another.

4. Diffuser shroud PIV cycle water hole experiment

4.1. Introduction to experimental equipment

As shown in Fig. 10, the experimental setup includes a circulating water tank, a PIV measurement system and a power control system. The circulating water tank mainly consists of an inlet tank, a contraction section, an

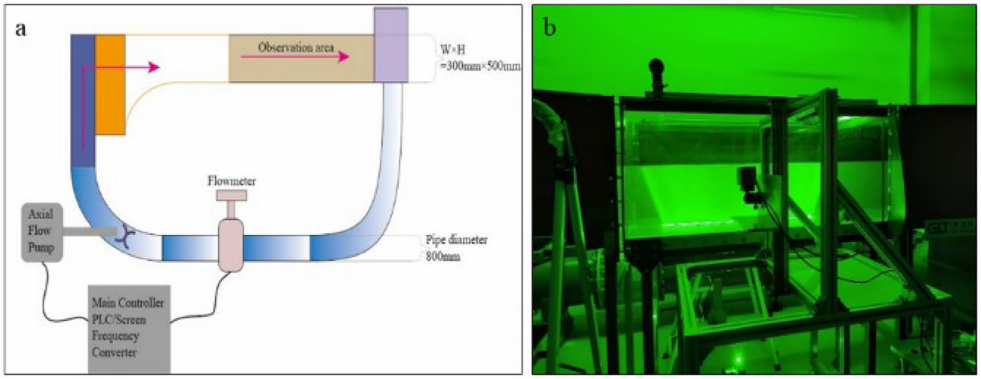

Fig. 10. (a) structural layout diagram of the PIV circulating water hole; (b) laser emission measurements.

experimental section, an expansion section, an outlet tank, pipes, an electromagnetic flow meter, a water pump and other components.

4.2. Experimental procedure

This paper first measured the flow velocity of the experimental section by means of an LS300-A flowmeter. The result shows 0.723 m/s, with an error of 3% within a controllable range. Therefore, it can be determined that the circulation tank and the flow meter have a good reliability.

The working flow velocity was set to 0.7 m/s and the flow field velocities were measured separately for the different types of diffuser shroud on the centerline. As there are fluctuations in the velocity of the flow controlled, the velocity of the flow field near the diffuser shroud is measured before measuring the velocity of the flow field away from the diffuser shroud. After measuring the flow velocity at the entrance to the water hole, the flow velocity at each point on the centerline of the diffuser shroud is measured by means of a flow velocity meter according to the flow field velocimetry experimental protocol. The experimental procedure is shown in Fig. 11.

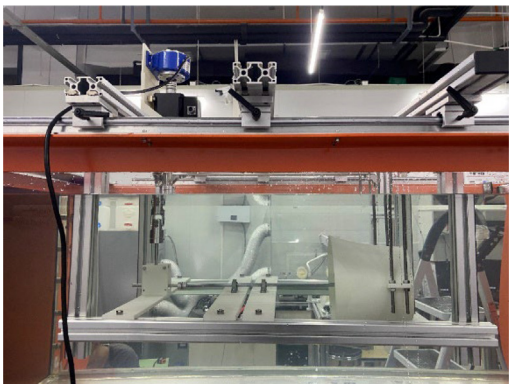

Fig. 11. Measuring the effect of diffuser shroud speed increase through the PIV recirculating water hole.

4.3. Experimental results

For the basic diffuser shroud, the flow rate growth rates on the centerline of the diffuser are compared and analyzed for four different diffusion opening angles ($a = 7°, 9°, 10°, 15°$) at a flow velocity of 0.7 m/s, an inlet diameter of $D = 170$ mm and a length to diameter ratio of $D/L = 2$ for the diffuser. This is shown in Fig. 12(a–d). These four sets of experimental data are in general agreement with the simulation results. The diffuser has the

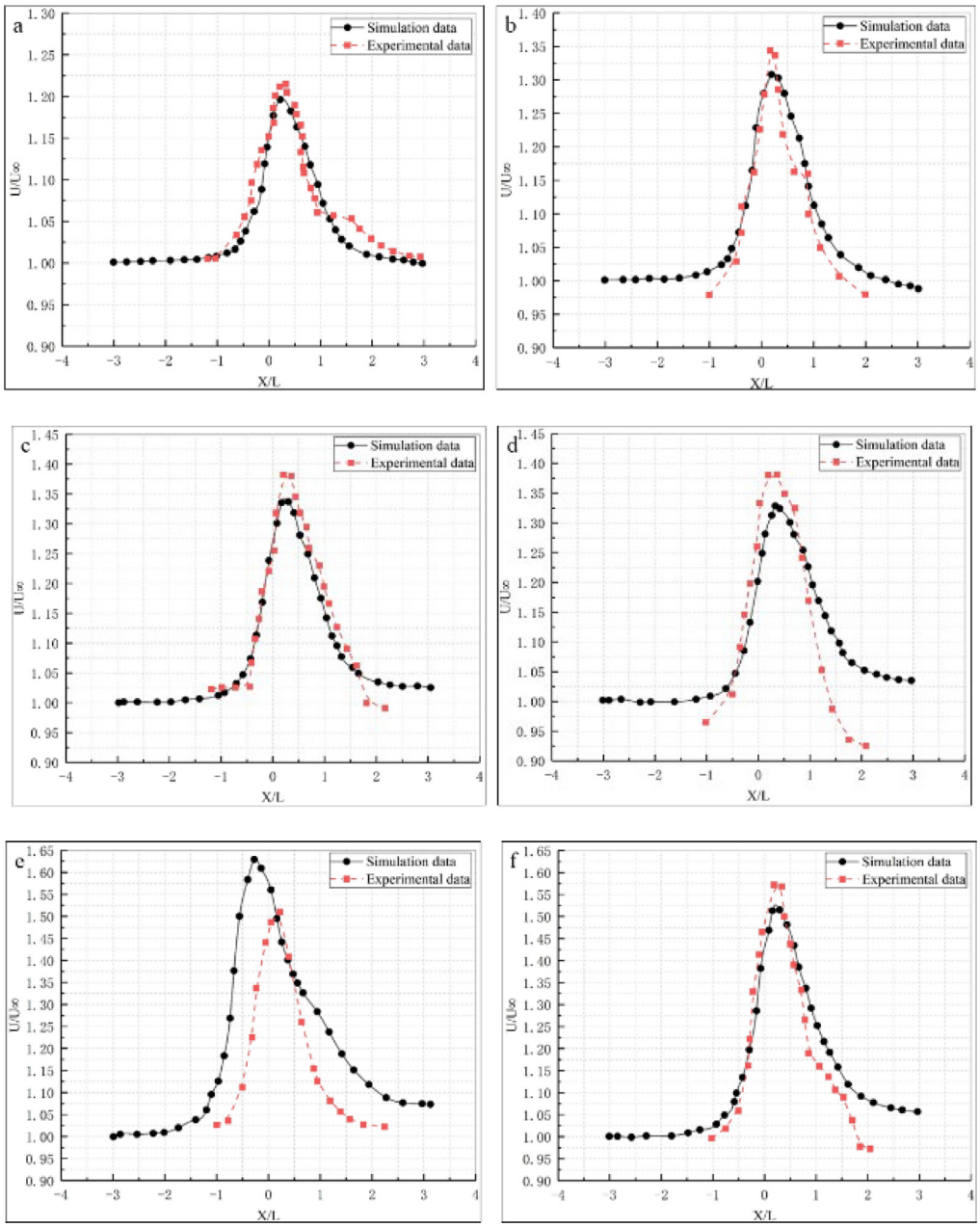

Fig. 12. Comparison of experimental and simulation results. (a) the velocity at diffusion opening angle 7°; (b) the velocity at diffusion opening angle 9°; (c) the velocity at diffusion opening angle 10°; (d) the velocity at diffusion opening angle 15°; (e) the velocity at NACA2412; (f) the velocity at NACA4412.

best velocity increase effect on the flow field when the diffuser diffusion opening angle is 15°. The experimentally measured velocity increase coefficient can reach 1.39, and the best velocity increase position X/L = 0.45.

For the wing section diffuser, the flow rate growth rate on the centerline of two different wing section diffusers (NACA4412, NACA2412) were measured experimentally under the conditions that the inlet diameter D = 170 mm and the length-to-diameter ratio D/L = 2 was fixed, as shown in Fig. 12(e) and (f). The experimental data can verify the simulation results of the airfoil section diffuser. The experimental results show that the growth rate coefficient

of the NACA4412 wing section diffuser reaches about 1.58 and the optimum growth rate position X/L = 0.50, which is an improvement of about 13.67% compared to the fundamental diffuser.

5. Conclusion

(1) Under low-flow current kinetic conditions, the flow velocity is critical to the energy capture efficiency of an ocean current energy turbine. diffuser shroud can increase the flow velocity in the local flow field, thereby increasing the energy capture efficiency of the OCT.

(2) In the CFD flow field simulation, the basic diffuser shroud can achieve a velocity increase factor of 1.49 for the velocity flow field, and the optimum location for the velocity increase is X/L = 0.245. The airfoil section diffuser shroud can achieve a velocity increase factor of 1.63 for the velocity flow field, and the optimum location for the velocity increase is X/L = 0.221.

(3) During experiments in the PIV circulation water hole, the basic diffuser shroud can achieve a velocity increase factor of 1.39 for the velocity field, with the optimum location for the increase being X/L = 0.450. The diffuser shroud with an airfoil section can achieve a velocity increase factor of 1.58 for the velocity field, with the optimum location for the increase being X/L = 0.500.

(4) Through the experimental study of the effect of the diffuser shroud on the velocity increase of the flow field, overall, the experimental measurement data and simulation data fit with an average error of less than 4%.

(5) In this paper, through the design and optimization of the aggregated flow augmentation for low-flow ocean current energy, we can achieve efficient power generation from low-flow ocean current energy and improve the capture efficiency and utilization of ocean current energy. In the future, we will further study the effect of multiple sets of ocean current wake to further improve the energy capture efficiency of distributed ocean current turbines.

Declaration of competing interest

The authors declare no conflict of interest.

Data availability

No data was used for the research described in the article

Acknowledgments

This project was supported by the equipment pre-research and sharing technology project of the equipment development department of China Military Commission (No. 41421080302).

References

[1] Cai T, Dong M, Chen K, Gong T. Methods of participating power spot market bidding and settlement for renewable energy systems. Energy Rep 2022;8:7764–72. http://dx.doi.org/10.1016/j.egyr.2022.05.291.

[2] Muangjai P, Wongsapai W, Bunchuaidee R, Tridech N, Ritkrerkkrai C, Damrongsak D, Bhuridej O. Estimation of marginal abatement subsidization cost of renewable energy for power generation in thailand. Energy Rep 2022;8:528–35. http://dx.doi.org/10.1016/j.egyr.2022.05.197.

[3] Hu H, Xue W, Jiang P, Li Y. Bibliometric analysis for ocean renewable energy: An comprehensive review for hotspots, frontiers, and emerging trends. Renew Sustain Energy Rev 2022;167:112739. http://dx.doi.org/10.1016/j.rser.2022.112739.

[4] Ko D-H, Ge Y, Park J-S, Liu L, Ma C, Chen F, Peng J, Kang S-K, Yi J-H, Liu W. A comparative study of laws and policies on supporting marine energy development in China and Korea. Mar Policy 2022;141:105057. http://dx.doi.org/10.1016/j.marpol.2022.105057.

[5] Saboori B, Gholipour HF, Rasoulinezhad E, Ranjbar O. Renewable energy sources and unemployment rate: Evidence from the US states. Energy Policy 2022;168:113155. http://dx.doi.org/10.1016/j.enpol.2022.113155.

[6] Solarin SA, Bello MO, Tiwari AK. The impact of technological innovation on renewable energy production: accounting for the roles of economic and environmental factors using a method of moments quantile regression. Heliyon 2022;8:e09913. http://dx.doi.org/10.1016/j.heliyon.2022.e09913.

[7] Li B, Chen W, Li J, Liu J, Shi P. Integrated monitoring and assessments of marine energy for a small uninhabited island. Energy Rep 2022;8:63–72. http://dx.doi.org/10.1016/j.egyr.2022.01.114.

[8] van der Schoor T, Scholtens B. Power to the people: Local community initiatives and the transition to sustainable energy. Renew Sustain Energy Rev 2015;43:666–75. http://dx.doi.org/10.1016/j.rser.2014.10.089.

[9] Zhao T, Xu M, Xiao X, Ma Y, Li Z, Wang ZL. Recent progress in blue energy harvesting for powering distributed sensors in ocean. Nano Energy 2021;88:106199. http://dx.doi.org/10.1016/j.nanoen.2021.106199.
[10] Bahaj AS, Batten WM, McCann G. Experimental verifications of numerical predictions for the hydrodynamic performance of horizontal axis marine current turbines. Renew Energy 2007. http://dx.doi.org/10.1016/j.renene.2007.10.001.
[11] Batten WM, Bahaj AS, Molland AF, Chaplin JR. The prediction of the hydrodynamic performance of marine current turbines. Renew Energy 2008. http://dx.doi.org/10.1016/j.renene.2007.05.043.
[12] Hudson SM. Energy harvesting of cathodic protection currents in subsea and marine structures for wireless sensor power and communication. Appl Energy 2022;(8).
[13] Karaalioglu MS. Performance prediction of cavitating marine current turbine by BEMT based on CFD. Ocean Eng 2022;(20).
[14] Zhang Y, Zang W, Zheng J, Cappietti L, Zhang J, Zheng Y, FernandezRodriguez E. The influence of waves propagating with the current on the wake of a tidal stream turbine. Appl Energy 2021;290:116729. http://dx.doi.org/10.1016/j.apenergy.2021.116729.
[15] Göltenbott U, Ohya Y, Yoshida S, Jamieson P. Aerodynamic interaction of diffuser augmented wind turbines in multi-rotor systems. Renew Energy 2017;112:25–34. http://dx.doi.org/10.1016/j.renene.2017.05.014.
[16] Wang W-X, Matsubara T, Hu J, Odahara S, Nagai T, Karasutani T, Ohya Y. Experimental investigation into the influence of the flanged diffuser on the dynamic behavior of CFRP blade of a shrouded wind turbine. Renew Energy 2015;78:386–97. http://dx.doi.org/10.1016/j.renene.2015.01.028.
[17] Alkhabbaz A, Yang H-S, Tongphong W, Lee Y-H. Impact of compact diffuser shroud on wind turbine aerodynamic performance: CFD and experimental investigations. Int J Mech Sci 2022;216:106978. http://dx.doi.org/10.1016/j.ijmecsci.2021.106978.
[18] Lipian M, Dobrev I, Karczewski M, Massouh F, Jozwik K. Small wind turbine augmentation: Experimental investigations of shrouded- and twin-rotor wind turbine systems. Energy 2019;186:115855. http://dx.doi.org/10.1016/j.energy.2019.115855.